Chemical Physics xxx (2012) xxx–xxx

Contents lists available at SciVerse ScienceDirect

Chemical Physics

journal homepage: www.elsevier.com/locate/chemphys

Recent attoclock measurements of strong field ionization

Adrian N. Pfeiffer *, Claudio Cirelli, Mathias Smolarski, Ursula Keller

Physics Department, ETH Zurich, 8093 Zurich, Switzerland

ARTICLE INFO

Article history:
Available online xxxx

Keywords:
The attoclock measures time by electron streaking with elliptically polarized light
Precision measurements reveal details about the laser-induced tunneling current flow
Multielectron effects play an important role when the polarizability is large
Double ionization experiments show evidence of novel electron correlation mechanisms

ABSTRACT

The attoclock is a powerful, new, and unconventional experimental tool to study fundamental attosecond dynamics on an atomic scale. We have demonstrated the first attoclock with the goal to measure the tunneling delay time in laser-induced ionization of helium and argon atoms, with surprising results. It was found that the time delay in tunneling is zero for helium and argon atoms within the experimental uncertainties of a few 10's of attoseconds. Furthermore we showed that the single active electron approximation is not sufficient even for atoms such as argon and the parent-ion interaction is much more complex than normally assumed. For double ionization of argon we found again surprising results because the ionization time of the first electron is in good agreement with the predictions, whereas the ionization of the second electron occurs significantly earlier than predicted and the two electrons exhibit some unexpected correlation.

Published by Elsevier B.V.

1. Introduction

The key process underlying attosecond physics is strong field ionization by femtosecond laser pulses [1–3]. The strong electric field of the laser pulse bends the binding potential of the ion such that the electron is separated from the continuum by a potential barrier, through which it can escape by tunneling. Depending on the phase of the external electric field, the tunneled electron may recollide with the parent ion. Possible processes upon recollision are scattering to higher energies, which leads to an extended plateau in the photoelectron spectrum [3,4], or scattering with other electrons leading to double or multiple ionization [5]. Another possibility is that the electron recombines with the parent ion, which leads to the emission of high-energy photons. This is the so-called process of high-order harmonic generation (HHG) [4,6–9], which is the fundamental process for the generation of attosecond pulses [10,11].

Attosecond pulses and laser-controlled electron trajectories have been used for direct imaging of the electric field of a laser pulse [12], to observe quantum path control and interference within the HHG process [13,14], to image molecular orbitals [15], and to probe molecular dynamics on an ultrafast time scale [16–18]. In this sense progress in attoscience, aiming at the resolution of the dynamics of the electron motion on its natural timescale, requires a detailed understanding of tunnel ionization.

In attosecond streaking [19,20], a weak attosecond pulse ionizes an atomic [21], molecular [22] or solid target [23]. The attosecond pulse is overlaid with a relatively intense femtosecond infrared laser pulse. The electron gains a final energy that depends on the instant it appears in the continuum where it is accelerated by the femtosecond pulse. Therefore the photoelectron spectrum depends on the delay between the atto- and the femtosecond pulse. Attosecond streaking experiments have addressed very fundamental questions in quantum mechanics such as: how fast can light remove a bound electron from an atom [21,24,25] or from a surface [23]?

The attoclock is a powerful, new, and unconventional tool to study fundamental attosecond dynamics on an atomic scale. The attoclock is also an attosecond streaking technique but here the time reference is given by a close-to-circularly polarized laser field. In this way it is possible to obtain attosecond time resolution by employing a femtosecond pulse [26]. However, the attoclock technique could also be used with attosecond pulses. The close-to-circularly polarized laser field with the rotating electric field vector gives the time reference similar to the hands of a clock and is based on the definition of "time" by "counting cycles and/or fractions of cycles". In case of a "normal clock" the hour hand rotates the full cycle over 360° in 12 h, the minute hand in 60 min and the second hand in 60 s. Thus, the faster the rotating hand the more accurate is the time measurement. In case of the attoclock, the "minute hand" is the rotating electric field vector of the laser pulse which rotates a full cycle in 2.7 fs (for a center wavelength of 800 nm).

For the attoclock we measure the laser pulse polarization, and the momentum vectors of ions and electrons in coincidence, using

* Corresponding author. Present address: Ultrafast X-ray Science Laboratory, Chemical Sciences Division, Lawrence Berkeley National Laboratory, Berkeley, CA 94720, USA. Tel.: +1 510 643 5464; fax: +1 510 643 1961.
E-mail address: apfeiff@phys.ethz.ch (A.N. Pfeiffer).

0301-0104/$ - see front matter Published by Elsevier B.V.
doi:10.1016/j.chemphys.2012.02.005

"COLd Target Recoil Ion Momentum Spectroscopy" (COLTRIMS) [27,28]. Depending on the data acquisition time, an accuracy of a few attoseconds can be achieved because the measurement is based on a peak search for the exact angle at which the highest electron and ion count rate are observed [24]. The attoclock cycle, the "time zero", the laser polarization and the exact time evolution of the streaking laser field are fully characterized independently. In addition, using both clockwise and anti-clockwise polarized pulses we can minimize systematic errors in the angular streaking.

Because of the close-to-circular polarization, the probability for re-scattering of the liberated electron with the parent ion is very low and the ionization event is very well isolated. After the tunneling event, the liberated electron is considered to propagate classically in the combined laser field and the potential of the parent ion, so that the instant of ionization can be mapped to the angle of the final momentum of the electron in the polarization plane, measured with the COLTRIMS apparatus. The ion and electron momenta are measured in coincidence, which means that they can be grouped according to their atom of origin. This opens up the possibility to explore correlations between the involved particles.

2. Outline

In this paper we review recent experiments that made use of the attoclock technique. First it is discussed how the attoclock provides timings on a coarse and on a fine scale, similar to the hour and the minute hand of a watch face. This principle can be used to measure the "ionization time", i.e., the time zero of the electron trajectory. We found that the ionization time of the first electron in double ionization of argon is in good agreement with the model predictions, whereas the ionization of the second electron occurs significantly earlier than predicted [29].

A comparison of the maximum in the distribution of the electron emission angle to the angular orientation of the polarization ellipse has allowed us to resolve the timing of the ionization process. We measured the time in between the maximum of the electric field and the maximum of the ionization rate, referred to as "tunneling delay time". We found that the tunneling delay time is zero within the experimental uncertainties of a few 10's of attoseconds.

A modified semi-classical model was introduced which explained our experimental results taking into account a more complex electron parent-ion interaction with multi-electron effects and the Stark shift during the streaking process [30]. The tunnel exit points calculated with the new model are generally larger than in the standard model, and the threshold intensity for over-the-barrier ionization is increased substantially.

3. Initial conditions for the semi-classical model

A very simplified and very useful model to describe ionization in an intense laser pulse is the so-called semi-classical model [4,31,32]. This semi-classical picture uses a scalar potential for the laser field interaction, which corresponds to the length gauge in the dipole approximation. This is generally considered to be a valid picture for a center wavelength of around 800 nm and the laser intensities discussed here (e.g. shaded area in [33]). This semi-classical model in the length gauge then results in two distinct steps in the ionization process with an elliptically polarized laser field: the first step is the tunnel event which liberates the electron from the bound state in the atom (i.e. a clear quantum mechanical event) and the second step is the classical trajectory of the liberated electron in the combined potential of the parent ion and the strong laser field.

The electric field of the laser pulse given by

$$\mathbf{F}(t) = \begin{pmatrix} F_x(t) \\ F_y(t) \end{pmatrix} = \frac{f(t)\sqrt{I}}{\sqrt{\varepsilon^2+1}} \begin{pmatrix} \cos(\omega t + \varphi_{\mathrm{CEO}}) \\ \varepsilon \sin(\omega t + \varphi_{\mathrm{CEO}}) \end{pmatrix} \tag{1}$$

where I is the peak intensity, $f(t)$ is the normalized field envelope, ε is the ellipticity, and φ_{CEO} is the carrier-envelope-offset (CEO) phase [34]. With this convention, the xy-plane is the polarization plane and the major polarization axis is oriented along the x-axis. Atomic units are used throughout the paper and the atomic unit of intensity is $3.509 \times 10^{16}\,\mathrm{W/cm^2}$.

In the following electron motion the laser field exerts the dominant force, but also the Coulomb attraction by the parent ion acts on the electron. However, the electron is pulled far away from the parent ion within a fraction of the optical cycle and the Coulomb attraction becomes a small perturbation compared to the laser field. In the simplest approximation the Coulomb field is neglected after ionization. In this case, the final momentum after the laser pulse of an electron that was liberated at a time t is approximately given by:

$$\begin{pmatrix} p_x(t) \\ p_y(t) \end{pmatrix} \approx \frac{f(t)\sqrt{I}}{\omega\sqrt{\varepsilon^2+1}} \begin{pmatrix} \sin(\omega t + \varphi_{\mathrm{CEO}}) \\ -\varepsilon \cos(\omega t + \varphi_{\mathrm{CEO}}) \end{pmatrix} \tag{2}$$

Even though the simple approach of neglecting the interaction of the liberated electron with its parent ion potential is very successful for many purposes, effects have been discovered revealing that the Coulomb force influences the electron trajectory in the continuum or even under the barrier [35]. These effects include Coulomb focusing [36,37], Coulomb asymmetry in above-threshold ionization [38] and the recently discovered low energy structure at mid-infrared laser wavelengths [39,40]. More recently we clearly demonstrated that the Coulomb potential alone is not a sufficient correction. We even need to take into account multi-electron effects in an atom such as Argon. Even more complicated interactions are expected for molecules and surfaces [30].

To include the influence of the parent ion potential, the electron trajectory $\mathbf{r}$ is calculated by solving numerically the equation of motion in the combined potential of the laser pulse and the ion potential. The difference of this trajectory compared to the electron trajectory in the laser field only is mainly a change in the final electron emission direction (Fig. 1). This angular offset θ in helium is dominated by the Coulomb correction. This Coulomb correction is especially sensitive to the ion-electron attraction at the beginning of the electron trajectory. In general however this angular offset θ is much more complicated and not fully explored and understood to date [30].

The transition from the tunneling process into a classically moving particle raises serious issues both from a conceptual definition and from a measurement point of view. The link between the first and the second step of the semi-classical model, i.e. between tunneling and classical propagation, is still debated. Specifying the initial conditions for the classical electron movement after the tunnel event provides this link. The initial conditions for the electron trajectory are the ionization time, the tunneling delay time, the exit of the tunnel, and the initial momentum of the electron. In addition for the electron trajectory dynamics we need to have a clear model for the combined potential of the parent ion and the strong laser field. In a first approximation of the semi-classical picture we assume a zero initial momentum of the electron at the exit of the tunnel. This approximation can be further refined with an initial electron wavepacket spread [41]. This could be verified experimentally [42,43]. A discussion about the starting time and starting point for the electron trajectory follows in the next sections.

Please cite this article in press as: A.N. Pfeiffer et al., Chem. Phys. (2012), doi:10.1016/j.chemphys.2012.02.005

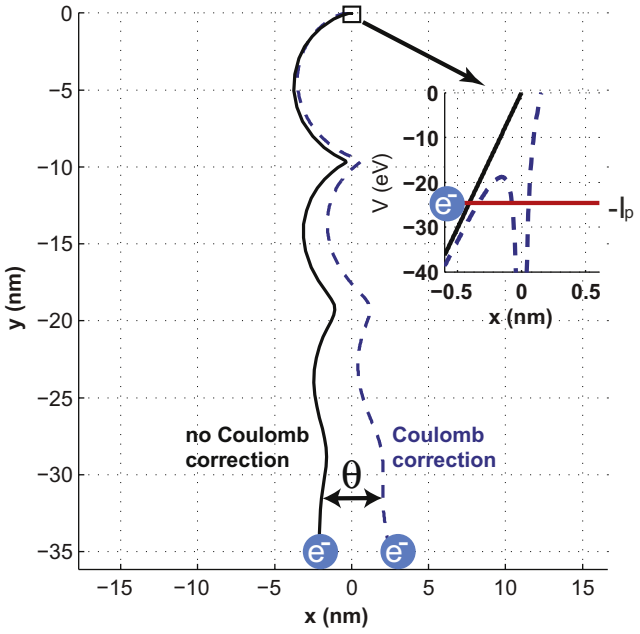

Fig. 1. Semi-classical model. Classical electron trajectory following the tunnel event calculated in the potential of the laser field (black solid) and the combined potential of the laser field and the parent ion (blue dashed). The Coulomb correction angle θ is the angle in between the final directions. Inset: The effective potential of an atom in a strong laser field in the length gauge (blue dashed) results from the superposition of the Coulomb potential and the scalar laser potential (black solid). An electron bound with the ionization potential I_p can escape from the atom by tunneling through a classically forbidden barrier.

4. Experimental setup of the attoclock

For the experiments presented here, we used to different laser pulses: either a laser pulse with a duration of about 30 fs produced by a Ti:Sapphire based laser system, or a laser pulse with a duration between 5 and 7 fs generated by compressing the 30-fs pulse with a two-stage filament compressor [44]. Intensity control is achieved differently for the two pulses: the intensity of the 30-fs pulse was varied by a rotating half-wave plate in front of a polarizer, the intensity of the short pulse by means of a motorized iris.

Close-to-circularly polarized laser pulses ($\varepsilon \approx 0.8 - 0.95$) are generated by propagating the laser pulses through a broadband quarter wave plate. Laser pulses with higher ellipticity cannot easily be obtained due to the residual wavelength dependence of the quarter wave plate, and are for most attoclock experiments also not demanded. Within the scope of this paper, the polarization state of a laser pulse is defined by the angular orientation of the polarization ellipse and the ellipticity. For the measurement of the polarization state, a polarizer was rotated while recording the power throughput with a power meter before the COLTRIMS measurement was taken. The power throughput as a function of polarizer angle allows extracting the value for the ellipticity and the angle of the polarization ellipse from a curve fitting function.

The laser pulses are focused into a supersonic jet of atoms inside a COLTRIMS [27,28] setup. A homogeneous electric field and a homogeneous magnetic field are applied along the spectrometer axis. The charged particles created at the intersection between the laser focus and the gas jet are guided to time- and position sensitive detectors by the spectrometer fields, facilitating the calculation of the initial vector momenta of the atomic fragments after the laser pulse has passed.

The ion and electron momenta are measured in coincidence. The distribution of ($\mathbf{p}_{\text{Ion}} + \mathbf{p}_{\text{Electron}}$) must peak at zero due to momentum conservation. In the case of double ionization, the momenta of the doubly charged ion and the two electrons need to be measured. From momentum conservation follows the condition $\mathbf{p}_{\text{Ion}} + \mathbf{p}_{\text{Electron1}} + \mathbf{p}_{\text{Electron2}} = 0$, see Fig. 2. The probability of ionization per laser shot must be kept well below one for these coincidence detections, to assure that most of the detected particles stem from the same parent atom.

5. Attoclock measurements

5.1. Measurement of the ionization time

The ionization time measurements make use of the semi-classical model. Within this model, it is possible to define the ionization time as the moment in time when the classical electron trajectory starts [29]. This is the moment when the electron is liberated into an unbound state and is also referred to as the electron release time. To calculate the ionization time from the measured momentum, it is useful to transform the momentum given by Eq. (2) into (ellipticity corrected) polar coordinates:

$$p_r(t) \equiv \sqrt{(\varepsilon^2+1)p_x^2 + \left(\frac{\varepsilon^2+1}{\varepsilon^2}\right)p_y^2} \approx \frac{f(t)\sqrt{I}}{\omega} \tag{3}$$

$$p_\varphi(t) \equiv \tan^{-1}\left(\frac{(-\sqrt{\varepsilon^2+1}/\varepsilon)p_y}{\sqrt{\varepsilon^2+1}p_x}\right) \approx \omega t + \varphi_{\text{CEO}} \tag{4}$$

The radial momentum is proportional to the field envelope and thus changes slowly with time. For the calculation of the polar coordinates, it is crucial to know the ellipticity and the angular orientation of the polarization ellipse. The time evolution of the polar momentum coordinates is depicted in Fig. 3. The radial momentum coordinate changes slowly with time, such that it allows a coarse ionization time measurement. After this coarse measurement, the accuracy of the time measurement can be increased by exploiting the information encoded in the radial coordinate.

We have applied this method to measure the ionization times in double ionization in argon. With depletion the averaged ionization times are shifted to the beginning of the laser pulse with increasing intensities for both the first and the second ionization step (Fig. 4).

A mechanism that dominates double ionization by linearly polarized laser pulses over a wide intensity regime is recollision of the first emitted electron with its parent ion [45]. By using close-to-circularly polarized laser pulses, this mechanism is not avoided in general [46], but probably greatly suppressed for noble gas atoms. Therefore it was hitherto believed that the two successive ionization steps would occur by field ionization without mutual electron interaction. If we compare the measurement of the ionization times to calculations based on the semi-classical model in the independent electron approximation, using quasi-static ionization rates [47], we find that the first ionization time is in good agreement with theory, whereas the second electron is ionized earlier than expected (Fig. 4).

Furthermore there are correlations in the emission directions of the electrons [48]. There is a tendency that the two electrons are emitted preferentially into the same (parallel electron emission) or into opposite hemispheres (antiparallel electron emission), depending on the laser intensity (Fig. 5).

The physical mechanism that is responsible for these observations remains unclear, but the oscillatory behavior of electron correlation as a function of intensity could be reproduced by a classical ensemble simulation [49]. Strong field ionization of multielectron atoms holds many aspects that go beyond the semi-classical model in its simplest form. Examples of multielectron phenomena in strong field ionization are the position of the

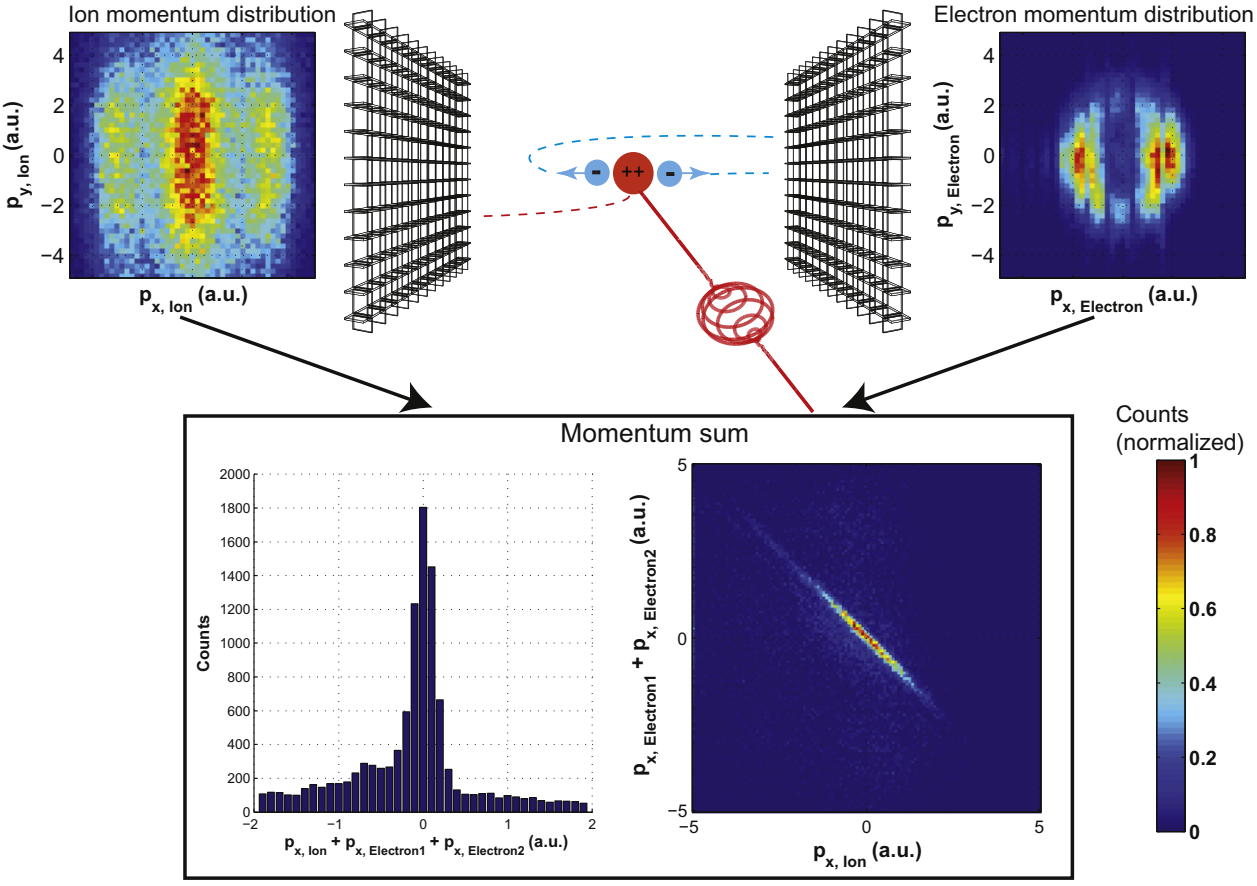

Fig. 2. COLTRIMS coincidence measurements. The spectrometer fields guide the charged particles to detectors, which allows the calculation of the momenta. Due to momentum conservation, the sum of the ion momentum and the two electron momenta (lower panel, adapted from [29]) must equal zero if the detected particles stem from double ionization of a single atom. The spectra are integrated over the acquired intensity range, which is up to 3.5 PW/cm^2 in this case.

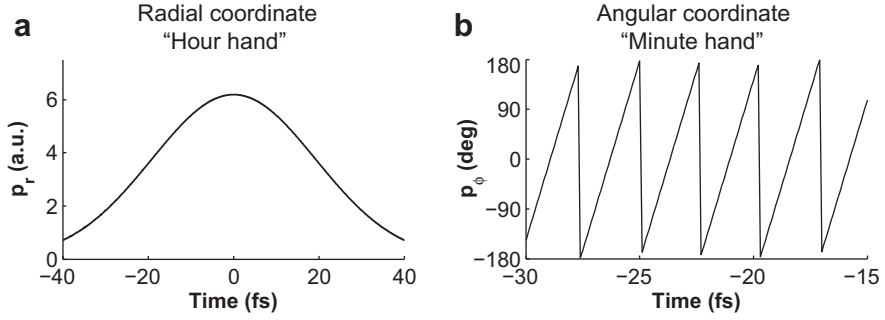

Fig. 3. Time measurement with the attoclock. (a) The time evolution of the radial momentum p_r (hour hand of the attoclock) is rather slow, but allows an unambiguous momentum-to-time mapping if restricted to the first half of the laser pulse. (b) The time evolution of the angular coordinate $p\varphi$ is fast and therefore allows a mapping to time with higher precision. Laser parameters: intensity = 4.5 PW/cm^2, FWHM = 33 fs.

tunnel exit [30] and the electron hole movement in the valence shell of the ion [50]. There are other phenomena that remain not understood up to now, like the degree of orbital alignment after tunnel ionization [51,52].

5.2. Measurement of the tunneling delay time

The tunneling delay time is defined as the time delay in between the maximum of the instantaneous laser intensity and the maximum of the ionization rate [24].

The averaged momentum distribution that is caused by circularly polarized laser pulses without CEO phase stabilization looks like a torus in the polarization plane. The reference that is necessary for the comparison of the electric field to the ion momenta is provided by the slight ellipticity of the laser pulse. In the statistical average over many laser shots, the highest field amplitude is reached when the electric field vector points into the direction of the major axis of the polarization ellipse in case that the CEO phase is not stabilized [26]. This causes two maxima to appear in the torus of the momentum distribution (Fig. 6). The angle of the maximum in the toroidal momentum distribution is extracted from the COLTRIMS data; the angle of the major polarization ellipse can be determined by polarimetry.

The angle in between the major axis of the polarization ellipse and the maxima of the ion momentum distribution is caused by two different effects. The first effect is a potential angular

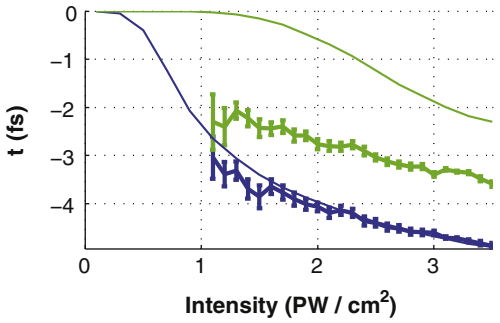

Fig. 4. Electron release times in strong field double ionization. The average of the first (blue) and second (green) ionization time as a function of intensity for a 7-fs laser pulse. The vertical axis gives the timing relative to the laser pulse, such that zero designates the peak of the pulse. The solid lines show the prediction of the independent electron model. Adapted from [29].

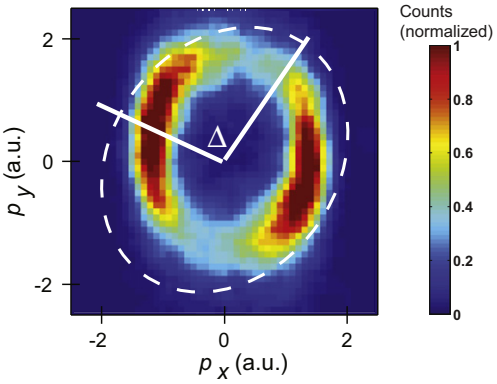

Fig. 6. Momentum distribution arising from close-to-circularly polarized laser pulses. The polarization ellipse is depicted by the white dashed line. The white solid lines indicate the maxima of the polarization ellipse and the ion momentum distribution. Adapted from [24].

difference between the maximum of the electric laser field, which induces the highest ionization rate, and the direction of the laser field when the electron exits the tunnel. This corresponds to the tunneling delay time. The second effect is the streaking in the electric field of the laser and the parent ion, which causes an offset of about 90° (Figs. 1 and 6). By calculating the streaking angle, we could determine the angle caused by the tunneling delay time and found it to be zero within the experimental uncertainty of about 12 as for helium in an intensity range from 0.23 to 0.35 PW/cm^2.

The result of zero tunneling delay time could recently be extended to a much wider intensity regime, and also to argon atoms [30]. The result is especially interesting in comparison to the delay in one-photon photoemission that is found by attosecond streaking. The photoelectrons originating from the 2p shell in neon are delayed by 21 ± 5 as with respect to photoelectrons from the 2s shell [21]. However, only about half of that delay is explained by current theory [21,25,53–58].

5.3. Measurement of the tunnel exit

The Coulomb correction can be used as a probe for the initial starting point of the electron trajectory. The offset angle θ is very sensitive to a change in the tunnel exit points and to the potential energy landscape in which the tunneled electron moves. The geometry of the electron current flow, the Stark shift of the energy levels, and the induced dipole contribution of the bound electrons all significantly influence the starting point of the classical trajectory and the potential during electron propagation [30] (Fig. 7). We monitored the evolution of the offset angle θ as a function of laser intensity for helium and argon. No significant change of θ is observed for helium over the investigated intensity range, while argon exhibits a monotonic downwards trend of θ with increasing intensity (Fig. 8).

In helium the Stark shifts and the induced dipole modifications are negligible, because of the very small polarizabilities of the atom and positively charged ion. It is the separation in parabolic coordinates that leads to a plateau in the θ dependence on intensity, rather than the weak monotonic increase of the Cartesian-based semi-classical model.

Time-dependent Schrödinger equation (TDSE) simulations [59] are in agreement with our argon data but could only be performed over a limited intensity range without serious numerical problems. The standard semi-classical model, consisting of an initial tunneling step and subsequent classical propagation of the electronic trajectories, formulated in Cartesian coordinates, fails to reproduce the experimental trend in the offset angle for argon, predicting a maximum at an intensity close to the over-the-barrier (OBI) ionization.

Going to a model based on parabolic coordinates [60,61] improves the agreement: the trend is monotonic, even though it is upwards. The additional inclusions of Stark shifts (larger binding energies), and even more, of multi-electron effect through the increase of the barrier due to the ionic induced dipole, become

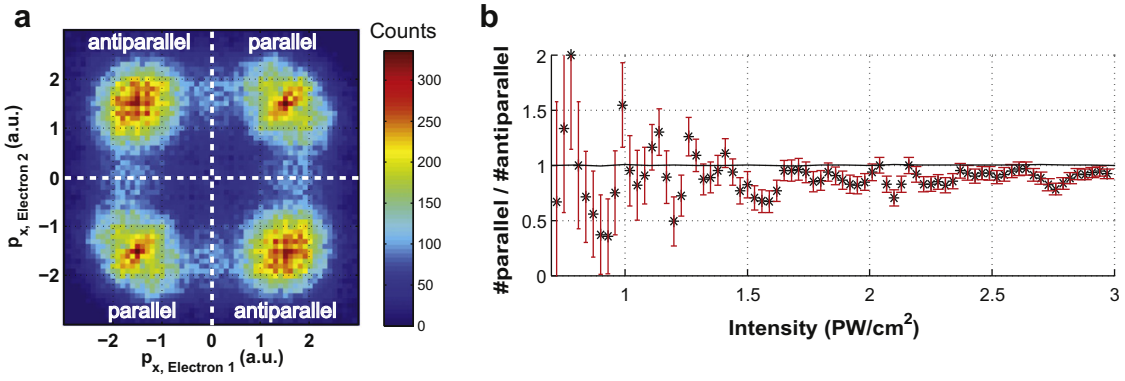

Fig. 5. Electron correlation in strong field double ionization by close-to-circular polarization. (a) Momentum correlation between both electrons for double ionization of argon by a 7-fs laser pulse. Horizontal axis: momentum component of one electron along the minor axis of the polarization ellipse, vertical axis: same momentum component of the second electron. The spectrum is integrated over the intensity range 0–3 PW/cm^2. (b) Ratio of parallel to anti-parallel electron emission for 7-fs (a) and 33-fs pulses. Adapted from [48].

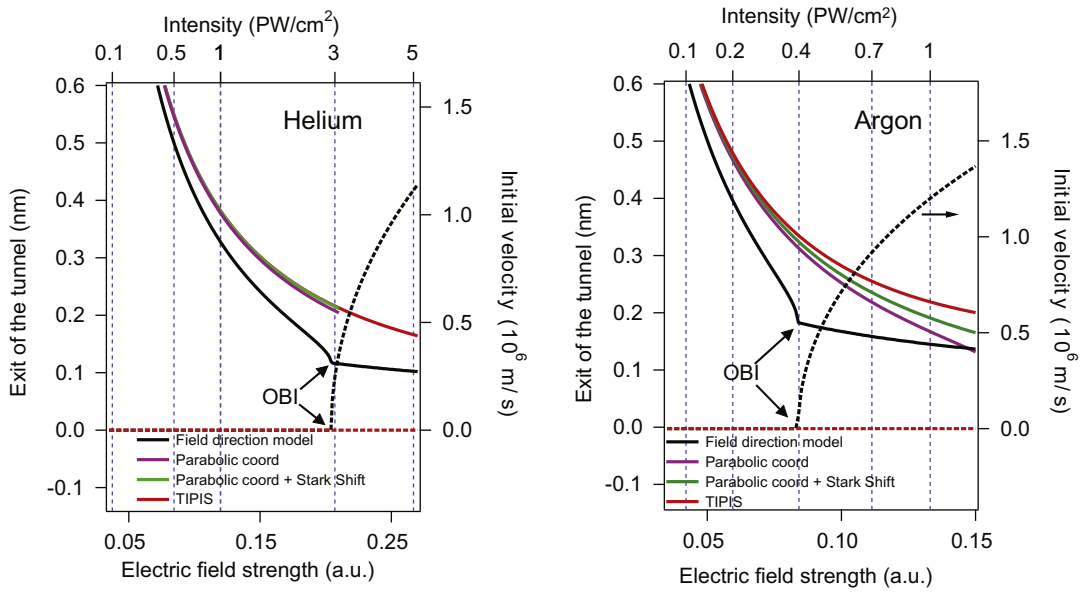

Fig. 7. Tunnel exits for helium and argon as a function of field strength. The position where the electron appears in the continuum after tunnel ionization, as schematically drawn in the inset of Fig. 1 for the field direction model, depends on the model that is used. See [30] for a detailed discussion of the models and the respective calculation of the tunnel exit. Adapted from [30].

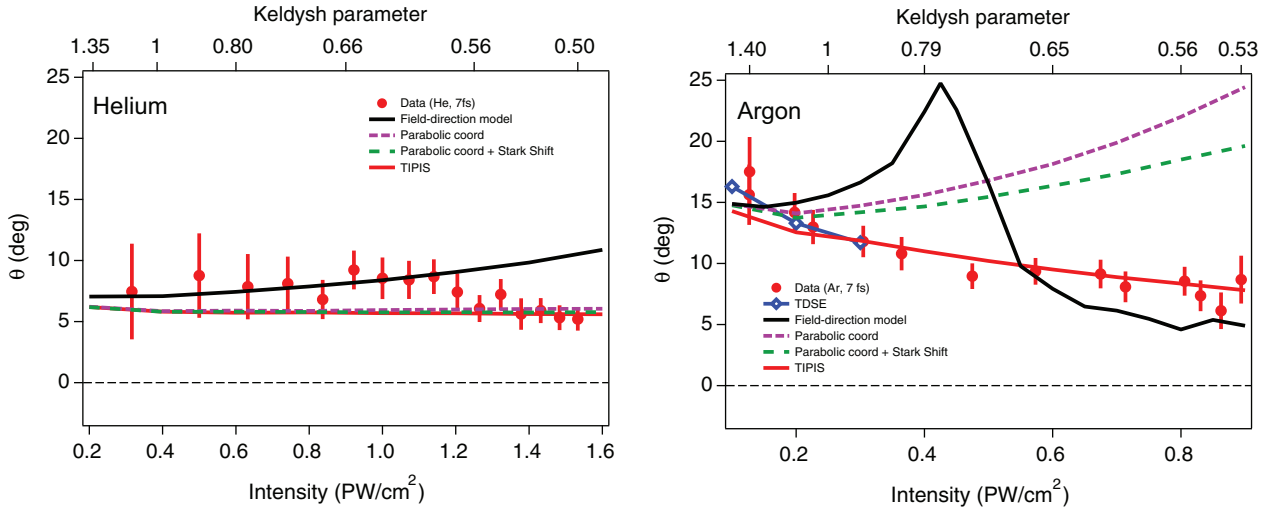

Fig. 8. Angular offset for helium and argon. (a) Angular offset θ, obtained from ion momentum distribution, measured in Helium as a function of laser intensity; (b) same observable obtained from electron momentum distribution measured in Argon, shown together with the TDSE simulations. In both plots different model curves are shown as well. For the calculation of the model curves, an ensemble of classical electron trajectories distributed according to a strong field ionization rate [47] is calculated starting from the exit of the tunnel shown in Fig. 7. Adapted from [30].

decisive for the decrease of θ with increasing intensity in the case of argon.

In collaboration with Lars B. Madsen and Darko Dimitrovski we have introduced a new modified semi-classical tunneling model that includes multi-electron effects. The model correctly describes the observed attosecond ionization dynamics, and changes important underlying physical parameters. We refer to this new model as TIPIS – Tunnel Ionization in Parabolic coordinates with Induced dipole and Stark shift [30].

6. Conclusion

For strong field single ionization, the potential of the parent ion was used as a probe for the kinematics of the electron. The influence of the ion potential is mostly subtle and therefore often neglected. Nevertheless it offers a unique opportunity, because the Coulomb field shows a high spatial dependence at the dimensions of the electron trajectory during the laser pulse, whereas the force of the laser acts uniformly at these dimensions. The tunneling delay time was found to be zero within the experimental uncertainties for helium and argon atoms. For the starting position of the electron after tunneling (the exit of the tunnel), it was found that multi-electron processes need to be taken into account. The extent to which they influence the tunneling dynamics is system dependent as shown here by the difference in helium and argon. Argon is much easier to polarize than helium and is therefore affected more strongly. The TIPIS model was introduced to describe the correct calculation of the tunnel exit.

In the case of strong field double ionization, surprising results were found. Up to now it was believed that the two ionization steps in close-to-circularly polarized laser pulses would occur

independently from each other. Nevertheless we found a strong correlation between the emission directions of the two electrons, and this correlation shows an oscillatory behavior when the intensity is increased. Furthermore, it was found that the ionization time of the second electron is earlier than predicted by the semi-classical model in the independent-electron approximation. These two findings seem to contradict the independent electron approximation.

7. Outlook

The attoclock is an extremely sensitive tool for the investigation of laser induced tunneling, one of the paradigms of modern strong-field and ultrafast science. The transition of the electron from a tunneling wavepacket into a classically moving particle remains a topic of intense discussions. The question about the initial wavepacket spread of the electron at the tunnel exit will be addressed in a future study [43]. At this point no attosecond pulses have been used for the attoclock measurements to resolve atomic ionization dynamics with a few 10's of attosecond timing accuracy. We plan additional interesting fundamental studies with non-degenerate attoclock measurements using attosecond XUV pulses and even terahertz fields. The possibilities are wide open.

The new insights gained for strong laser field ionization are of fundamental interest in itself, but they also have far reaching implications for the strong-field and ultrafast community. It is one of the goals to follow electron dynamics in real time and tunneling is the initial step in much of these investigations. We plan to extend the attoclock measurement to the mid-infrared spectral regime to explore the semi-classical model. In addition, it will be interesting to study larger molecular systems where much less is known compared to noble gases. Larger molecules are often polar, and much more polarizable then the noble gas atoms studied up to now. Hence the implications of the TIPIS model will be even more important to consider. At this point the multi-electron effects could be described with a static response and their properties have been studied with independent measurements. This means the multi-electron effects and relaxation processes have been much faster than our current timing accuracy of our attoclock. For larger targets we hope that the attoclock will resolve the multi-electron dynamics and provide new insight in novel electron correlations.

We further believe that the attoclock measurements revealed a new understanding which will have important implications on time measurement techniques in attoscience in general. The near infrared femtosecond pulse used in attosecond streaking experiments has the potential to polarize the atom and consequently lead to additional force terms like those identified in the work summarized here. These terms may influence the interpretation of streaking experiments.

Acknowledgments

All the work regarding the development of the attoclock technique was supported by the NCCR Quantum Photonics (NCCR QP) a research instruments of the Swiss National Science Foundation (SNSF), by the ETH Research Grant ETH-03 09-2 and by the SNSF R'Equip Grant 206021_128551/1. A special acknowledgment goes to our international collaborations with R. Dörner, A. Staudte, L.B. Madsen and D. Dimitrovski.

References

[1] F. Krausz, M. Ivanov, Rev. Mod. Phys. 81 (2009) 163.
[2] T. Brabec, F. Krausz, Rev. Mod. Phys. 72 (2000) 545.
[3] Z.H. Chang, P. Corkum, J. Opt. Soc. Am. B 27 (2010) B9.
[4] P.B. Corkum, Phys. Rev. Lett. 71 (1993) 1994.
[5] A. Becker, R. Dörner, R. Moshammer, J. Phys. B 38 (2005) S753.
[6] M. Ferray, A. L'Huillier, X.F. Li, L.A. Lompré, G. Mainfray, C. Manus, J. Phys. B: At. Mol. Opt. Phys. 21 (1988) L31.
[7] A. McPherson, G. Gibson, H. Jara, U. Johann, T.S. Luk, I.A. McIntyre, K. Boyer, C.K. Rhodes, J. Opt. Soc. Am. B 4 (1987) 595.
[8] A. L'Huillier, P. Balcou, Phys. Rev. Lett. 70 (1993) 774.
[9] J.L. Krause, K.J. Schafer, K.C. Kullander, Phys. Rev. Lett. 68 (1992) 3535.
[10] P.M. Paul, E.S. Toma, P. Breger, G. Mullot, F. Augé, P. Balcou, H.G. Muller, P. Agostini, Science 292 (2001) 1689.
[11] M. Hentschel, R. Kienberger, C. Spielmann, G.A. Reider, N. Milosevic, T. Brabec, P. Corkum, U. Heinzmann, M. Drescher, F. Krausz, Nature 414 (2001) 509.
[12] E. Goulielmakis, M. Uiberacker, R. Kienberger, A. Baltuska, V. Yakovlev, A. Scrinzi, T. Westerwalbesloh, U. Kleineberg, U. Heinzmann, M. Drescher, F. Krausz, Science 305 (2004) 1267.
[13] K.J. Schafer, M.B. Gaarde, A. Heinrich, J. Biegert, U. Keller, Phys. Rev. Lett. 92 (2004) 023003.
[14] A. Zaïr, M. Holler, A. Guandalini, F. Schapper, J. Biegert, L. Gallmann, U. Keller, A.S. Wyatt, A. Monmayrant, I.A. Walmsley, E. Cormier, T. Auguste, J.P. Caumes, P. Salières, Phys. Rev. Lett. 100 (2008) 143902.
[15] J. Itatani, J. Levesque, D. Zeidler, H. Niikura, H. Pépin, J.C. Kieffer, P.B. Corkum, D.M. Villeneuve, Nature 432 (2004) 867.
[16] H. Niikura, F. Legare, R. Hasbani, A.D. Bandrauk, M.Y. Ivanov, D.M. Villeneuve, P.B. Corkum, Nature 417 (2002) 917.
[17] H. Niikura, F. Légaré, R. Hasbani, M.Y. Ivanov, D.M. Villeneuve, P.B. Corkum, Nature 421 (2003) 826.
[18] S. Baker, J.S. Robinson, C.A. Haworth, H. Teng, R.A. Smith, C.C. Chirilă, M. Lein, J.W.G. Tisch, J.P. Marangos, Science 312 (2006) 424.
[19] M. Kitzler, N. Milosevic, A. Scrinzi, F. Krausz, T. Brabec, Phys. Rev. Lett. 88 (2002) 173904.
[20] J. Itatani, F. Quéré, G.L. Yudin, M.Y. Ivanov, F. Krausz, P.B. Corkum, Phys. Rev. Lett. 88 (2002).
[21] M. Schultze, M. Fiess, N. Karpowicz, J. Gagnon, M. Korbman, M. Hofstetter, S. Neppl, A.L. Cavalieri, Y. Komninos, T. Mercouris, C.A. Nicolaides, R. Pazourek, S. Nagele, J. Feist, J. Burgdorfer, A.M. Azzeer, R. Ernstorfer, R. Kienberger, U. Kleineberg, E. Goulielmakis, F. Krausz, V.S. Yakovlev, Science 328 (2010) 1658.
[22] G. Sansone, F. Kelkensberg, J.F. Perez-Torres, F. Morales, M.F. Kling, W. Siu, O. Ghafur, P. Johnsson, M. Swoboda, E. Benedetti, F. Ferrari, F. Lepine, J.L. Sanz-Vicario, S. Zherebtsov, I. Znakovskaya, A. L'Huillier, M.Y. Ivanov, M. Nisoli, F. Martın, M.J.J. Vrakking, Nature 465 (2010) 763.
[23] A.L. Cavalieri, N. Müller, T. Uphues, V.S. Yakovlev, A. Baltuska, B. Horvath, B. Schmidt, L. Blümel, R. Holzwarth, S. Hendel, M. Drescher, U. Kleineberg, P.M. Echenique, R. Kienberger, F. Krausz, U. Heinzmann, Nature 449 (2007) 1029.
[24] P. Eckle, A. Pfeiffer, C. Cirelli, A. Staudte, R. Dörner, H.G. Muller, M. Büttiker, U. Keller, Science 322 (2008) 1525.
[25] K. Klünder, J.M. Dahlström, M. Gisselbrecht, T. Fordell, M. Swoboda, D. Guenot, P. Johnsson, J. Caillat, J. Mauritsson, A. Maquet, R. Taïeb, A. L'Huillier, Phys. Rev. Lett. 106 (2011) 143002.
[26] P. Eckle, M. Smolarski, P. Schlup, J. Biegert, A. Staudte, M. Schöffler, H.G. Muller, R. Dörner, U. Keller, Nat. Phys. 4 (2008) 565.
[27] R. Dörner, V. Mergel, O. Jagutzki, L. Spielberger, J. Ullrich, R. Moshammer, H. Schmidt-Bocking, Phys. Rep. 330 (2000) 95.
[28] J. Ullrich, R. Mooshammer, A. Dorn, R. Dörner, L.P.H. Schmidt, H. Schmidt-Böcking, Rep. Prog. Phys. 66 (2003) 1463.
[29] A.N. Pfeiffer, C. Cirelli, M. Smolarski, R. Dörner, U. Keller, Nat. Phys. 7 (2011) 428.
[30] A.N. Pfeiffer, C. Cirelli, M. Smolarski, D. Dimitrovski, M. Abu-samha, L.B. Madsen, U. Keller, Nat. Phys. 8 (2012) 76.
[31] Kulander, K.C., Schafer, K.J., Krause, J.L. 1993. Dynamics of short-pulse excitation, ionization and harmonic conversion. In: Piraux, B., Lhuillier, A., Rzazewski, K. (Eds.), Super-Intense Laser-Atom Physics, 1993, pp. 95–110.
[32] K.J. Schafer, B. Yang, L.F. Dimauro, K.C. Kulander, Phys. Rev. Lett. 70 (1993) 1599.
[33] H.R. Reiss, Phys. Rev. Lett. 101 (2008) 043002.
[34] H.R. Telle, G. Steinmeyer, A.E. Dunlop, J. Stenger, D.H. Sutter, U. Keller, Appl. Phys. B 69 (1999) 327.
[35] S.V. Popruzhenko, G.G. Paulus, D. Bauer, Phys. Rev. A 77 (2008) 053409.
[36] D. Comtois, D. Zeidler, H. Pepin, J.C. Kieffer, D.M. Villeneuve, P.B. Corkum, J. Phys. B 38 (2005) 1923.
[37] T. Brabec, M.Y. Ivanov, P.B. Corkum, Phys. Rev. A 54 (1996) R2551.
[38] S.P. Goreslavski, G.G. Paulus, S.V. Popruzhenko, N.I. Shvetsov-Shilovski, Phys. Rev. Lett. 93 (2004) 233002.
[39] C.I. Blaga, F. Catoire, P. Colosimo, G.G. Paulus, H.G. Muller, P. Agostini, L.F. DiMauro, Nat. Phys. 5 (2009) 335.
[40] C.P. Liu, K.Z. Hatsagortsyan, Phys. Rev. Lett. 105 (2010).
[41] M.Y. Ivanov, M. Spanner, O. Smirnova, J. Mod. Opt. 52 (2005) 165.
[42] L. Arissian, C. Smeenk, F. Turner, C. Trallero, A.V. Sokolov, D.M. Villeneuve, A. Staudte, P.B. Corkum, Phys. Rev. Lett. 105 (2010).
[43] A.N. Pfeiffer, C. Cirelli, A.S. Landsman, M. Smolarski, D. Dimitrovski, L.B. Madsen, U. Keller, (2011), arXiv:1111.6033v2[physics.atom-ph].
[44] C.P. Hauri, W. Kornelis, F.W. Helbing, A. Heinrich, A. Courairon, A. Mysyrowicz, J. Biegert, U. Keller, Appl. Phys. B 79 (2004) 673.
[45] T. Weber, H. Giessen, M. Weckenbrock, G. Urbasch, A. Staudte, L. Spielberger, O. Jagutzki, V. Mergel, M. Vollmer, R. Dörner, Nature 405 (2000) 658.
[46] F. Mauger, C. Chandre, T. Uzer, Phys. Rev. Lett. 105 (2010) 083002.
[47] X.M. Tong, C.D. Lin, J. Phys. B 38 (2005) 2593.
[48] A.N. Pfeiffer, C. Cirelli, M. Smolarski, X. Wang, J.H. Eberly, R. Dörner, U. Keller, New J. Phys. 13 (2011) 093008.

[49] X. Wang, J.H. Eberly, 2011, arXiv:1102.0221v1.
[50] E. Goulielmakis, Z.-H. Loh, A. Wirth, R. Santra, N. Rohringer, V.S. Yakovlev, S. Zherebtsov, T. Pfeifer, A.M. Azzeer, M.F. Kling, S.R. Leone, F. Krausz, Nature 466 (2010) 739.
[51] R. Santra, V.S. Yakovlev, T. Pfeifer, Z.H. Loh, Phys. Rev. A 83 (2011) 033405.
[52] A. Fleischer, H.J. Wörner, L. Arissian, L.R. Liu, M. Meckel, A. Rippert, R. Dörner, D.M. Villeneuve, P.B. Corkum, A. Staudte, Phys. Rev. Lett. 107 (2011) 113003.
[53] J.C. Baggesen, L.B. Madsen, Phys. Rev. Lett. 104 (2010) 043602.
[54] S. Nagele, R. Pazourek, J. Feist, K. Doblhoff-Dier, C. Lemell, K. Tokesi, J. Burgdorfer, J. Phys. B: At. Mol. Opt. Phys. 44 (2011) 081001.
[55] C.H. Zhang, U. Thumm, Phys. Rev. A 82 (2010) 043405.
[56] A.S. Kheifets, I.A. Ivanov, Phys. Rev. Lett. 105 (2010) 233002.
[57] M. Ivanov, O. Smirnova, Phys. Rev. Lett. 107 (2011) 213605.
[58] L.R. Moore, M.A. Lysaght, J.S. Parker, H.W. van der Hart, K.T. Taylor, Phys. Rev. A 84 (2011) 061404.
[59] C.P.J. Martiny, M. Abu-Samha, L.B. Madsen, J. Phys. B 42 (2009) 161001.
[60] L.D. Landau, E.M. Lifschitz, Quantum Mechanics (Non-relativistic Theory), Oxford University Press, Oxford, 1958.
[61] C.Z. Bisgaard, L.B. Madsen, Am. J. Phys. 72 (2004) 249.

Please cite this article in press as: A.N. Pfeiffer et al., Chem. Phys. (2012), doi:10.1016/j.chemphys.2012.02.005